View metadata, citation and similar papers at core.ac.uk

brought to you by CORE

provided by Purdue E-Pubs

Purdue University

Purdue e-Pubs

International Refrigeration and Air Conditioning Conference

School of Mechanical Engineering

2021

Numerical Investigation of Carbon Dioxide and POE Oil Mixture Behavior in an Accumulator in Trans-critical Heat Pump Mode

Wenying Zhang
University of Illinois Urbana-Champaign, wenying3@illinois.edu

Pega Hrnjak
University of Illinois Urbana-Champaign

Follow this and additional works at: https://docs.lib.purdue.edu/iracc

Zhang, Wenying and Hrnjak, Pega, "Numerical Investigation of Carbon Dioxide and POE Oil Mixture Behavior in an Accumulator in Trans-critical Heat Pump Mode" (2021). *International Refrigeration and Air Conditioning Conference.* Paper 2112.
https://docs.lib.purdue.edu/iracc/2112

This document has been made available through Purdue e-Pubs, a service of the Purdue University Libraries. Please contact epubs@purdue.edu for additional information.
Complete proceedings may be acquired in print and on CD-ROM directly from the Ray W. Herrick Laboratories at https://engineering.purdue.edu/Herrick/Events/orderlit.html

Numerical investigation of carbon dioxide and POE oil mixture behavior in an accumulator in trans-critical heat pump mode

Wenying ZHANG[1], Pega HRNJAK[1,2]*

[1] ACRC, University of Illinois, Urbana, Illinois, USA

[2] Creative Thermal Solutions, Inc., Urbana, Illinois, USA

* Corresponding Author, pega@illinois.edu

ABSTRACT

Carbon dioxide is one of the most promising next-generation refrigerants for air-conditioning applications in electric vehicles because it has the advantages of good heating performance in cold climates and environmental-friendly properties. Nonetheless, there are limited data about reversible CO_2 heat pump systems for component-level performance and design. This paper focuses on the impact of different sizes of oil bleed hole on the liquid level and local pressure drop in the accumulator through CFD simulation. Also, we applied the experimental data obtained with a full CO_2 HP system for the boundary conditions and the measured properties of liquid POE-CO_2 for the materials in the simulation. The cases with different sizes of the oil bleed hole are investigated using the commercial computational fluid dynamics software Fluent. The results of this paper can be used to design the accumulator and improve 1-D models for reversible systems so that it can operate well in both air-conditioning and heat pump modes.

1. INTRODUCTION

In recent decades, electric vehicles (EVs) have become popular due to the growing concern of air pollution in cities. However, EVs require not only cooling in warm climates but also cabin-heating in cold climates due to the lack of waste heat from the Internal Combustion Engine (ICE). Reversible CO_2 heat pump systems can provide promising heating capacity and efficiency also at low ambient temperatures. Because CO_2 has a relatively high density compared to conventional refrigerants like R134a, the heating capacity drops less and there is no air-in-leak at the compressor suction point in extremely cold weathers.

On the other hand, the wide operating range of temperature of reversible heat pump systems brings another challenge for the reversible air-conditioning system: The heat pump system reliability and performance are significantly affected by the mass of the circulating refrigerant in the system. In air-conditioning (AC) mode, the system needs more refrigerant to operate in warm conditions due to the higher density of supercritical CO_2 at a higher operating pressure and the larger internal volume of the outdoor coil. On the contrary, the system requires much less refrigerant in heat pump (HP) mode. This refrigerant charge imbalance between AC and HP mode has been studied by Feng and Hrnjak (2017) using an R134a automotive heat pump system. They found that AC mode needs about 300 g more refrigerant than HP mode, and half of the imbalance was caused by the length difference of the liquid line while the rest was caused by heat exchanger size difference.

To solve this charge imbalance issue, researchers installed an accumulator, which is a vessel between the evaporator and compressor. The three main functions are to store extra refrigerants, to prevent large amounts of liquid from entering and damaging the compressor, and to provide sufficient oil supply to the compressor (Wang et al., 2005). The authors developed a steady-state 1-D model to simulate the behavior of accumulators and the performance of an R134a automobile system. The results show that accumulator dimensions, like the diameter of the oil bleed hole and diameter of the j-tube, affect the pressure drop and determine the suction quality at the compressor, and thus the coefficient of performance (COP) of the automotive AC system. Finlayson & Dickson (2005) investigated the liquid refrigerant storage in a transparent accumulator and compared the performance of an R134a automotive air-conditioning system with and without accumulator under idle, city, and high-way conditions. They described the different flooding phenomenon in idle and highway conditions: a calmer gas-liquid interface with a lower mass flow

rate and a more turbulent, foamy interface due to both higher flow rate and reduced space for separation. Raiser et al. (2006) introduced a 1-D accumulator model including a liquid-height-dependent refrigerant density model and validated the model experimentally with a CO_2 automotive air-conditioning system over a wide operating range. They conducted experiments to study the effects of mass flow rate, charge of refrigerant, and diameter of oil bleed hole on the outlet quality of the accumulator. More recently, Wang et al. (2019) presented the charge determination and refrigerant migration behavior of a CO_2 mobile air-conditioning system during start-up and shutdown using an accumulator with five observation mirrors. The authors also studied the effects of the diameter of the oil bleed hole and concluded that the cooling capacity and COP decreased as the diameter of the oil bleed-hole reduced from 1.0 to 0.5 mm. Zhang & Hrnjak (2020) built a 1-D simulation model of an integrated internal heat exchanger (IHX) and accumulator and validated the model with experimental data collected with different CO_2 mobile air-conditioner and heat pump systems. A sensitivity analysis was conducted numerically to study the effects of mass flow rate and operating temperature on the performance of the IHX and the liquid level in the accumulator. Results showed that the integrated IHX and accumulator provide more benefits in air-conditioning mode, especially the high ambient temperature conditions.

Overall, the researchers have proposed different 1-D models and conducted experiments to study the steady-state and transient behavior of accumulators in air-conditioning systems. However, the two-phase flow pattern, like vapor-liquid separation and jet-flow across the oil bleed-hole, and local pressure drop inside accumulator are rare in the open literature. Besides, there are inadequate data for heat pump application: the components are designed for air-conditioning mode, while the pressure in the accumulator and the transport properties of CO_2 and oil mixture can be different in HP mode. Thus, the purpose of this paper is to illustrate the flow characteristics of the vapor-liquid separation, present the local pressure drop, and provide more data for the 1-D model of accumulator in heat pump mode. Volume of Fluid (VOF) model in commercial software ANSYS Fluent is used to track the liquid-vapor interface.

2. Model and settings of the accumulator

2.1 Geometry and mesh of the accumulator

The geometry of this accumulator was presented in our previous paper (Zhang and Hrnjak, 2020). An updated section view of the schematic drawing of the integrated IHX and accumulator's 3-D model is shown in Figure 1 and the key dimensions of the accumulator model are listed in Table 1. The internal nylon cylinder serves as the accumulator (orange part in Figure 1). A helical tube is arranged in the gap between the accumulator and the stainless-steel housing shell and forms a force-fit contact. The red and blue arrows represent the high- and low-pressure streams and form a counter-flow heat exchanger in air-conditioning mode.

For the accumulator, the two-phase refrigerant from the evaporator outlet flows through the inlet tube at the top center and enters the accumulator. Then, the refrigerant flows radially on the top of the deflector, then downwards along the small gap between the deflector and the accumulator wall. Afterward, the refrigerant separates into vapor and liquid in the space above the liquid level. In the normal operating conditions, vapor and a small number of liquid droplets flow through the mesh oil filter on the top-end of the j-tube, while the majority of the liquid mixture flows through the oil bleed hole at the bottom-bend of the j-tube. Finally, the mixture of vapor and liquid flows upwards along the j-tube and exits the accumulator.

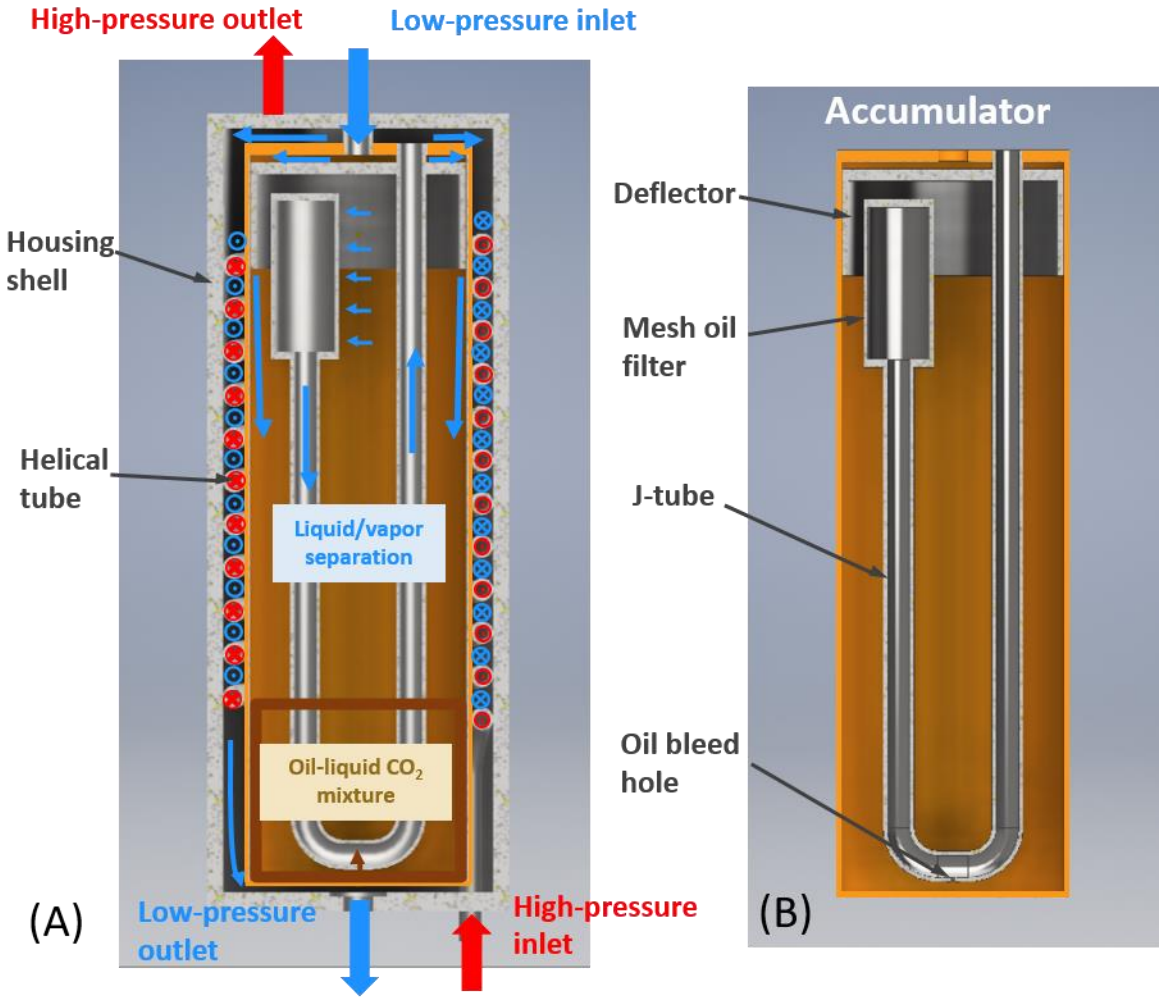

Figure 1: Section view of the 3-D model of (A) the integrated IHX and accumulator (B) accumulator only

Table 1: Key dimensions of the accumulator model

Internal diameter	**Internal height**	**Accumulator internal volume**	**J-tube internal diameter** D_j	**Oil bleed hole diameter** D_{BH}
51.7 mm	194 mm	407 mL	6 mm	1.0/ 1.2/ 1.4/ 1.6/ 1.8 mm

The simulation object in this paper is limited to the accumulator. Due to the complexity of the flow domain, tetrahedron mesh was generated and three layers of prism were added along the wall of the j-tube to capture the interface between the liquid and vapor phases and the flow behavior in the boundary layer.

For the mesh independence, we tried three sets of mesh files with 1.85, 4.30, and 9.99 million cells, and chose the 4.30 million cell mesh (0.78 million nodes) due to the balance between accuracy and calculation cost. Figure 2 shows the cross-section view of the mesh with 4.30 million cells and the details of the inlet of the j-tube and the oil bleed hole. For this set of mesh file, the minimum and maximum cell volume are 3.45e-15 and 6.59e-9 m^3.

Also, the minimum, maximum, and mean quality number of the mesh are 0.3081, 0.9996, and 0.7305 in the meshing software ANSYS ICEM. Also, the minimum skew value equals 0.3105. Generally, the quality of the mesh is good for our simulation.

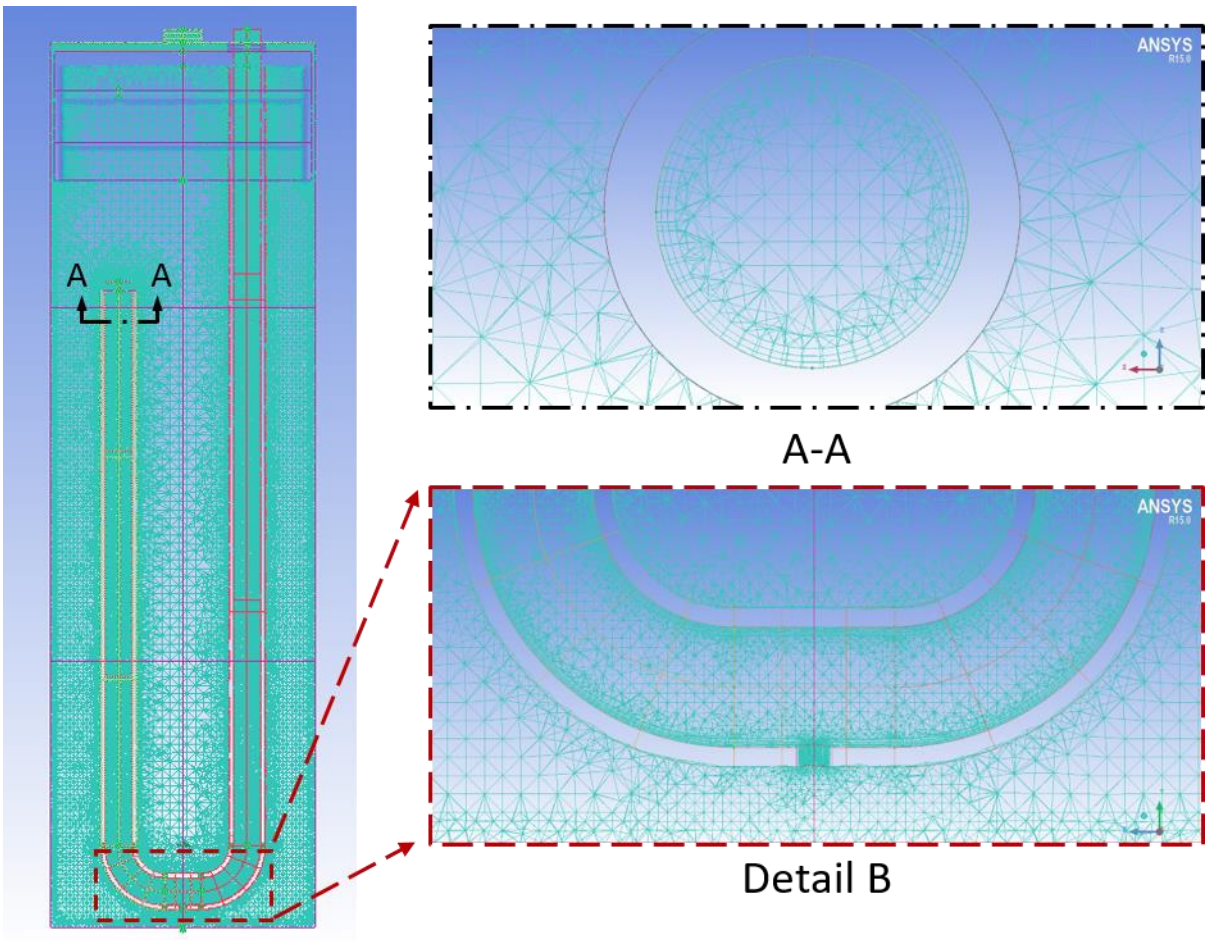

Figure 2: Section view of the volume mesh of the accumulator model and details of the prism on the wall of j-tube

2.2 VOF model and other settings

VOF (Volume of Fluid) model is a surface tracking method designed for multiple immiscible fluids where the interface is of interest. Compared with the Eulerian model, it solves one single set of momentum equations and reduces the calculation cost. Also, VOF model is more numerical-stable than the Eulerian model. Therefore, VOF model is used in this paper to simulate the flow characteristics.

For the turbulence model, realizable k-ε model and standard wall function are applied. The wall y-plus value ranges from 120 to 700 and agrees well with the requirement of the wall function. The materials include vapor CO_2 and the liquid mixture of POE oil and CO_2. The density, viscosity, and surface tension of the materials are from Seeton's dissertation (2009). The vapor phase is considered as the primary phase, while the liquid mixture is the second phase.

Besides, Pseudo Transient method is used for steady-state cases for better numerical stability. The convergence criterion of the simulation requires the residuals for all the variables are lower than 1e-2, the net mass flow rate of inlet and outlet is lower than 0.2 g/s, and the integration of the mass imbalance over the whole domain is lower than 1e-15.

2.3 Boundary and initial conditions

The mass flow rate boundary condition is adopted for the vapor and liquid inlets and the pressure boundary conditions are chosen for the outlet. For the initial condition, different liquid levels were iterated to converge faster for each geometry.

3. Results and discussion

3.1 Effects of the diameter of oil bleed hole on the liquid level

In this chapter, the effects of the diameter of the oil bleed hole on the liquid level and local pressure drop in steady state are analyzed. Figure 3 shows the simulation results for the liquid level and the streamlines inside the accumulator with different diameters of the oil bleed hole D_{BH}: 1.0, 1.2, 1.4, 1.6, and 1.8 mm. The red represents the liquid mixture of POE oil and liquid CO_2, while the blue represents the vapor CO_2. The boundary conditions of all the cases are the same: the inlet mass flow rates of vapor and liquid mixture are 26.80 and 3.43 g/s, while the oil circulating rate (OCR) is 2.0%. The static pressure at the exit is 3016 kPa. Gravity is in the negative y-direction. Those data are from the experimental data of a CO_2 HP system with the integrated accumulator and IHX in 0℃ condition.

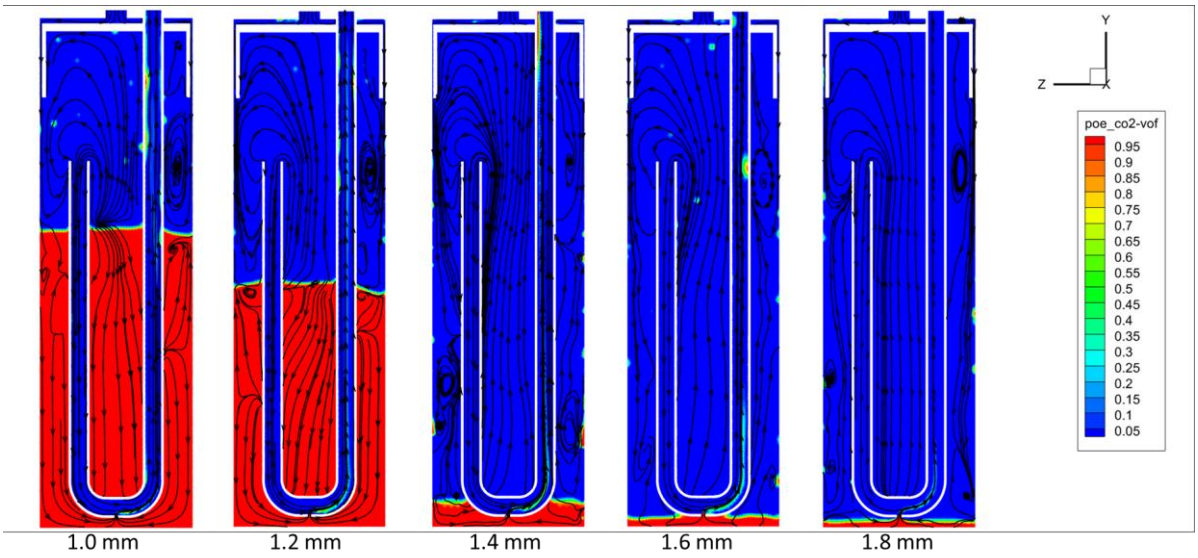

Figure 3: The volume fraction and streamlines inside accumulator with different sizes of oil bleed hole in y-z plane

The simulation results show that the liquid level in the accumulator decreases as the diameter of the oil bleed hole D_{BH} increases. The masses of the liquid mixture retained in the accumulator are 287.3, 236.9, 26.9, 10.7 and 8.4 g for D_{BH} are 1.0, 1.2, 1.4, 1.6, and 1.8 mm, respectively. Also, the mass-weighted average volume fraction was performed over the inlet surfaces of the j-tube at the top and the oil bleed hole at the bottom, as shown in Table 2. The volume fractions of the liquid mixture on the inlet surface of the j-tube at the top are lower than 1e-03 for almost all geometries, except for the 1.0 mm case. It can be concluded that for most of the cases only vapor enters the top inlet of the j-tube in steady-state in current HP operating condition. However, 1.6 mm might be too large for the diameter of the oil bleed hole because only a small amount of liquid mixture was retained in the accumulator and even some vapor flows through the bleed hole. As we can see in Table 2, the volume fractions of the liquid mixture on the inlet of the oil bleed hole are 8.64e-01 and 7.15e-01 for the 1.6 and 1.8 mm cases, while they are 1.00e+00, 9.79e-01, and 9.99e-01 for the 1.0, 1.2, and 1.4 mm cases, respectively.

Table 2: Mass-weighted average volume fraction on the inlet surfaces of j-tube and oil bleed hole (0 to 1: vapor to liquid)

Cases	liquid VOF on j-tube inlet	Liquid VOF on oil bleed hole inlet
1.0 mm	1.607682e-03	1.000000e+00
1.2 mm	2.360410e-05	9.789790e-01
1.4 mm	1.045071e-05	9.989258e-01
1.6 mm	5.640652e-04	8.646741e-01
1.8 mm	1.290481e-04	7.147483e-01

Figure 3 and Figure 4 also illustrate the streamlines of the two-phase flow in y-z and x-y planes. As we can see in Figure 3, the two-phase mixture falls along the wall and gradually separates, and only vapor flows upwards in the middle part of the accumulator. Due to the block of the right part of the j-tube, there are two local vortexes between it and the wall. This might reduce the separation efficiency when the liquid level increases. Thus, the geometry of the j-tube can be modified to smooth the flow and reduce the vortex. On the other hand, the liquid mixture flows downwards to the oil bleed hole after the separation. When the liquid part flows through the oil bleed hole, it forms a jet flow and is then bent by the perpendicular vapor flow. Then, as the two-phase mixture flows upwards along the j-tube, it first forms annular flow and breaks up into large drops due to the surface tension. Similar trends can be observed in Figure 4: vortexes are created in the bulk vapor under the deflector due to the two inversely vertical flows: upwards in the middle and downwards near the wall. In the 1.0- and 1.2-mm cases, vortexes exist in the bulk liquid, too.

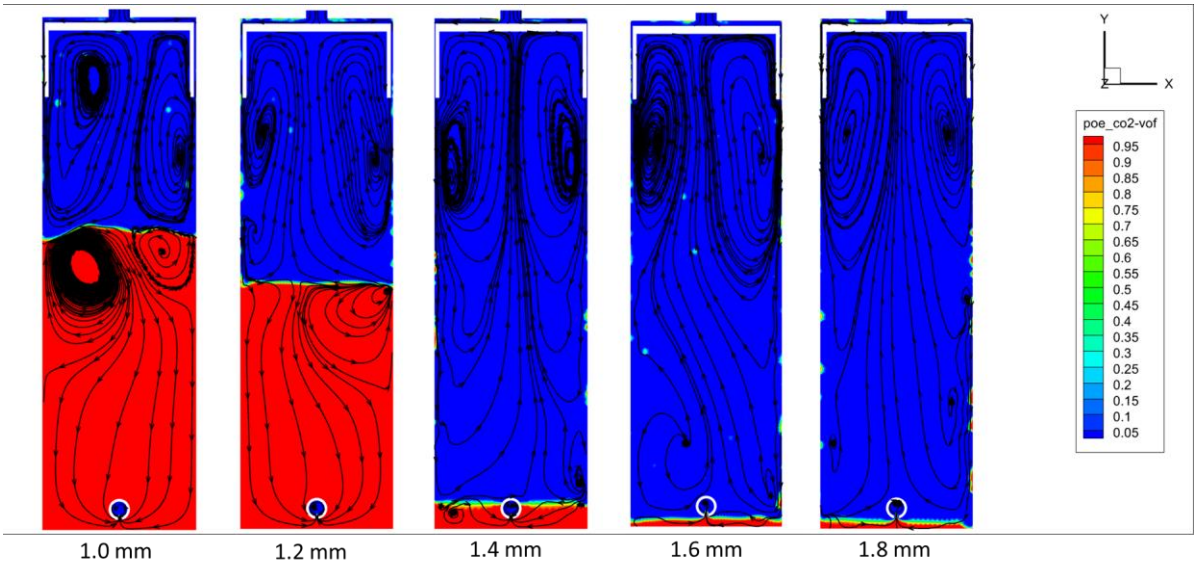

Figure 4: The volume fraction and streamlines inside accumulator with different sizes of oil bleed hole in x-y plane (perpendicular to the j-tube axis plane)

Figure 5 presents the flow pattern of the liquid mixture on the wall. The liquid flows through the thin gap between the deflector and the wall of the accumulator in a fingering shape. Later, the liquid breaks up into droplets due to the surface tension and the disturbance of the vapor flow.

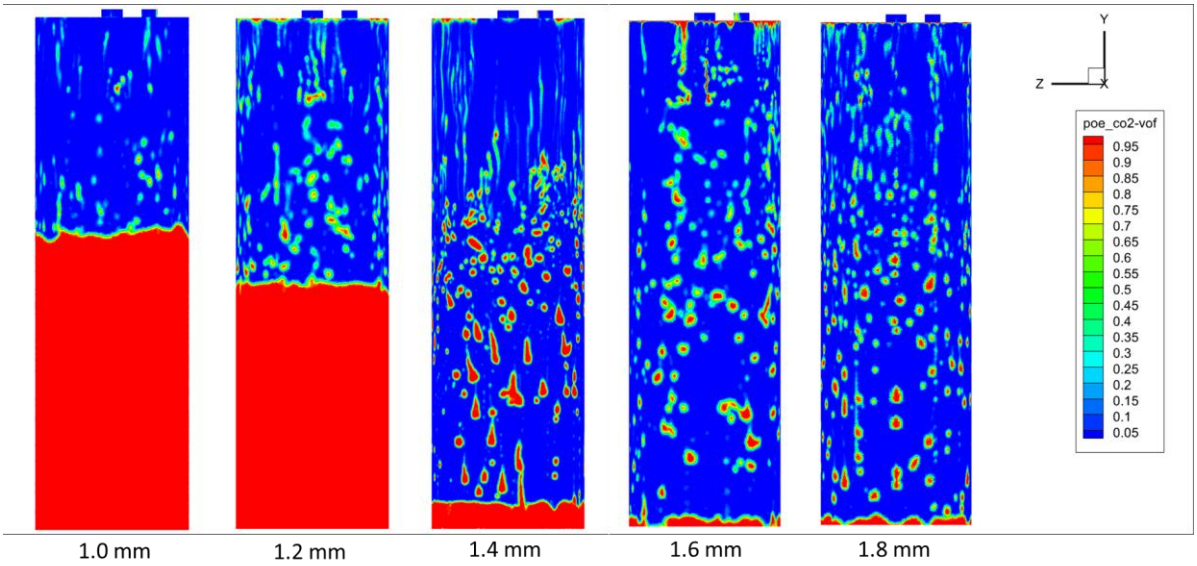

Figure 5: The volume fraction on the external wall of the accumulator with different sizes of oil bleed hole

3.2 Effects of the diameter of oil bleed hole on pressure drop

Figure 6 presents the static pressure in the accumulator with different sizes of the oil bleed hole in the y-z plane. The static pressure contours show that the major pressure drop occurs along the j-tube due to the high-velocity of the vapor and related friction. Also, there are other kinds of pressure drop due to bend, sudden contraction, and expansion. For example, when the two-phase impinging flow hits the top surface of the deflector, the velocity is forced to change the direction and creates a stagnation pressure drop of about 4 kPa. Another example is the pressure drop at the top inlet of the j-tube due to sudden contraction. As shown in Figure 7, the velocity of the bulk vapor in the accumulator is about 2 m/s, while it increases to 15 m/s as entering the j-tube. The static pressure drops by 10 to 13 kPa to compensate for this increase in dynamic pressure.

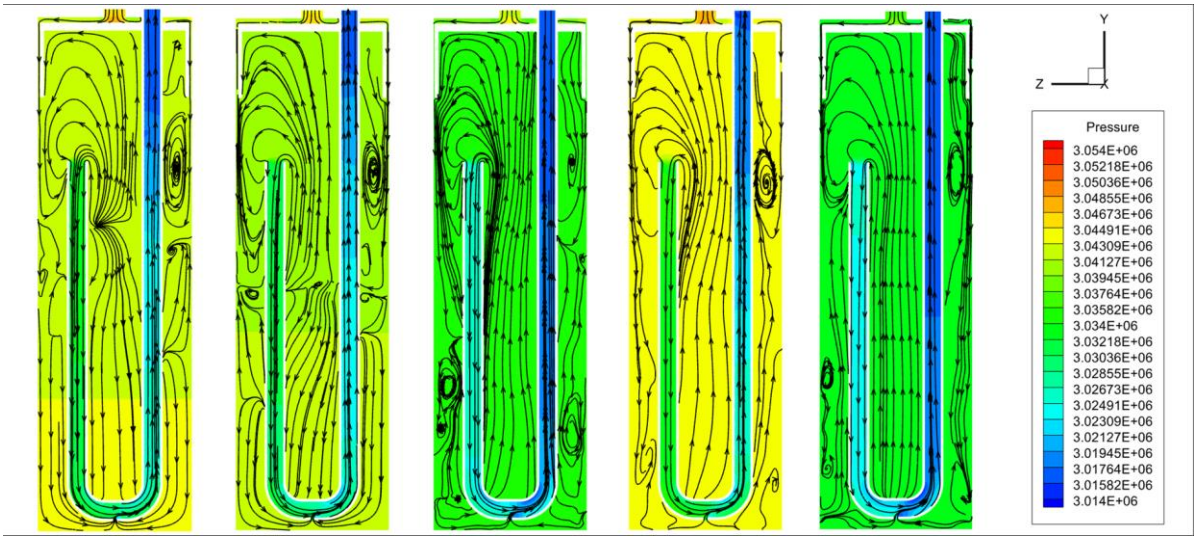

Figure 6: The static pressure inside the accumulator with different sizes of the oil bleed hole in y-z plane

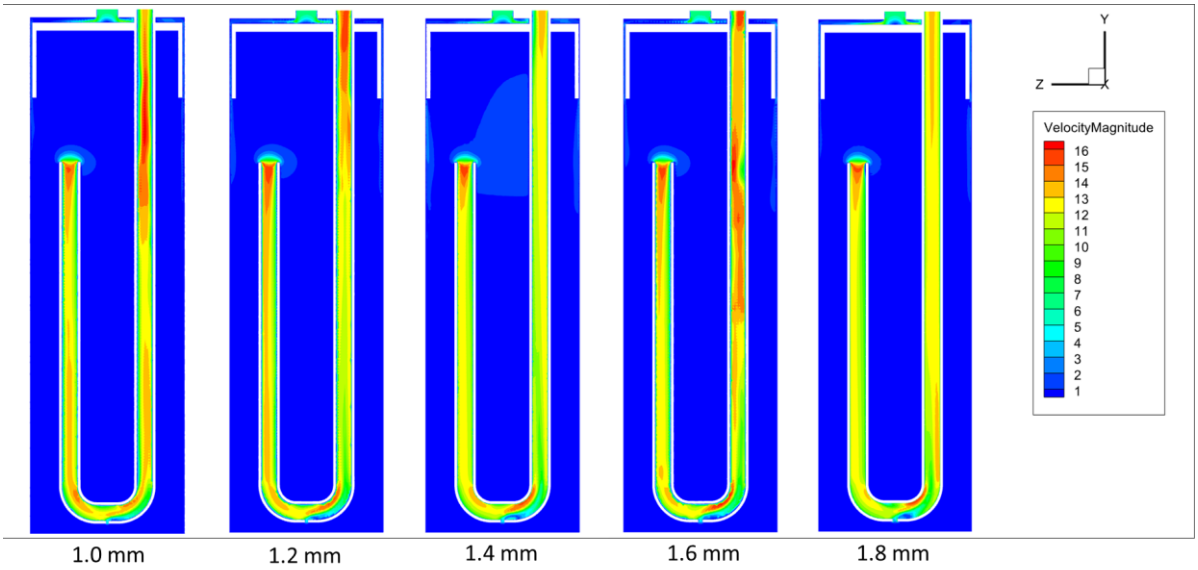

Figure 7: The velocity inside the accumulator with different sizes of the oil bleed hole in y-z plane

In the following section, the pressure drop across the oil bleed hole will be analyzed. Figure 8 presents the local pressure drop along a streamline across the oil bleed hole with different sizes. As shown earlier in Table 2, the local volume fractions of liquid at the inlet of the oil bleed hole are listed. Therefore, the mass flow rate across the oil bleed hole of all the cases can be calculated. Besides, the pressure drops across the oil bleed hole are listed in Table 3, so that the pressure drop coefficient *K* can be calculated using the following equation:

$$\Delta P = K \frac{1}{2} \rho V^2 \tag{1}$$

Where ΔP is the static pressure drop in Pa; ρ is the mass-weighted average density in kg/m^3, and *V* is the mass-weighted average velocity in the cross-section in m/s. It can be concluded that for a pure liquid mixture, the pressure drop coefficient varies a little from 2.57 to 2.69, while it is 1.51 for the two-phase flow with 1.8 mm D_{BH}. A sensitivity study can be conducted to summarize more general empirical values or equations for the local pressure drop coefficient of the oil bleed hole.

Table 3: Pressure drop across the oil bleed hole
(0 to 1: vapor to liquid)

Cases	Static pressure outside the BH [Pa]	Static pressure inside the BH [Pa]	Pressure drop [Pa]	Pressure drop coefficient
1.0 mm	3043383.89	3029639.74	13744.15	2.69
1.2 mm	3041927.02	3027545.48	14381.54	2.66
1.4 mm	3035605.26	3022319.11	13286.15	2.57
1.6 mm	3043574.53	3029294.71	14279.82	2.43
1.8 mm	3033093.93	3020568.81	12525.12	1.51

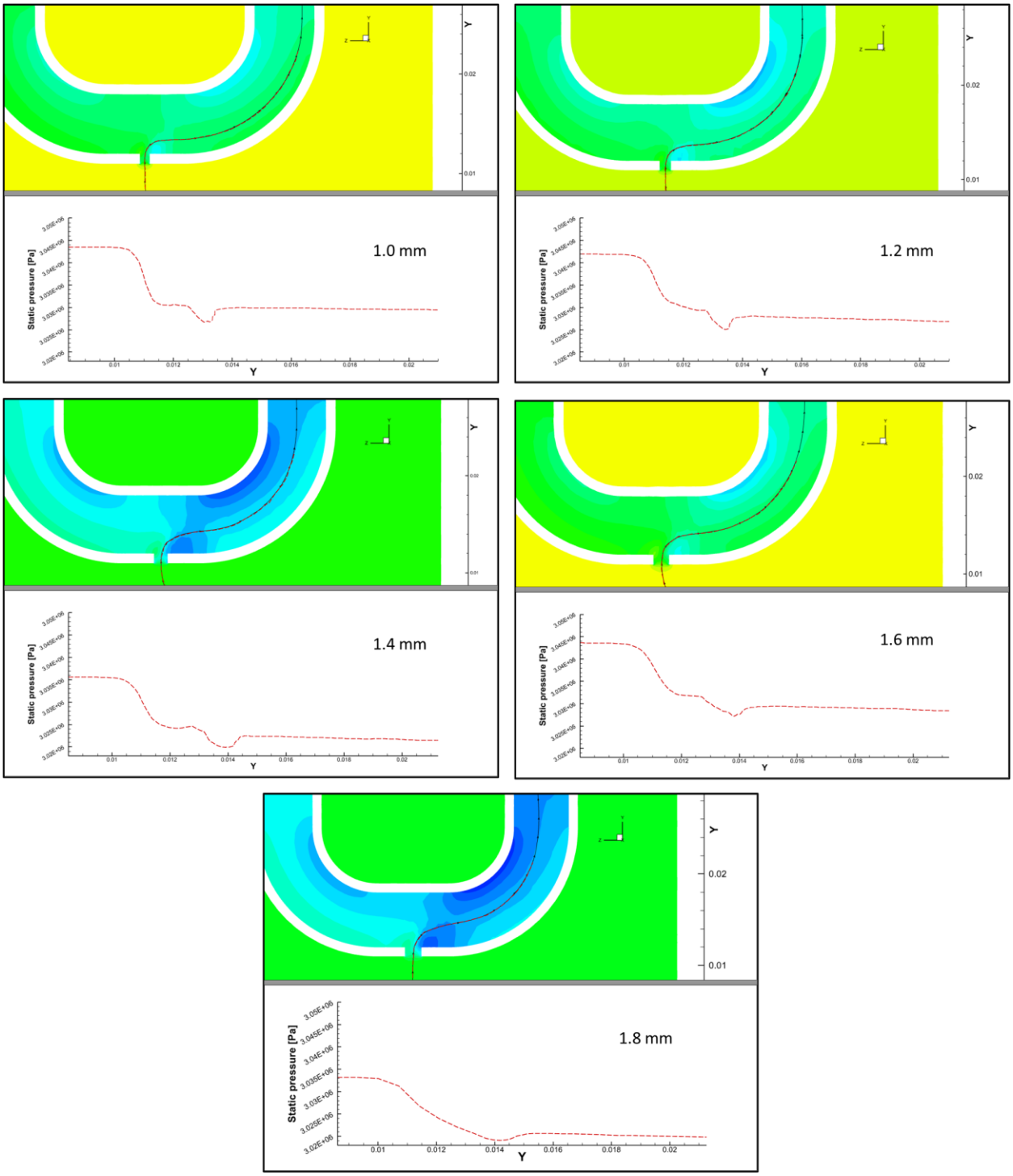

Figure 8: Pressure drop across the oil bleed hole with different sizes

4. CONCLUSIONS

This study investigates the flow characteristics of the two-phase CO_2 and POE mixture in the accumulator in a typical HP operating condition. The CFD simulation is conducted and the effects of different sizes of the oil bleed hole are analyzed.

- The liquid level in the accumulator decreases as the diameter of the oil bleed hole D_{BH} increases. The masses of the liquid mixture retained in the accumulator are 287.3, 236.9, 26.9, 10.7 and 8.4 g for D_{BH} are 1.0, 1.2, 1.4, 1.6, and 1.8 mm, respectively.
- Only vapor enters the top inlet of the j-tube for almost all geometries in current operating condition, except for the 1.0 mm case. Also, a 1.6 mm oil bleed hole is too large because only a small amount of liquid mixture was retained in the accumulator and even vapor CO_2 flows through the bleed hole.
- The flow pattern inside the accumulator is analyzed, which includes the vortexes of the vapor CO_2 and bulk liquid when the liquid level is high, the break-up of the jet flow of liquid mixture after the oil bleed hole, and the instability of the fingering flow along the wall.
- The static pressure contours show that the major pressure drop occurs along the j-tube due to the high-velocity of the vapor and related friction.
- Also, the pressure drop across the oil bleed hole and the pressure drop coefficients K are calculated for all cases: K varies little from 2.57 to 2.69 for pure liquid mixture, while it is 1.51 for two-phase flow with 1.8 mm D_{BH}.

NOMENCLATURE

D_{BH}	Diameter of oil bleed hole, m
D_j	Diameter of oil j-tube, m
K	Pressure drop coefficient, [-]
ΔP	Pressure drop, Pa
V	Mass-weighted average velocity, [m/s]
ρ	Mass-weighted average density, [kg/m^3]

Subscript

BH	oil bleed hole
j	j-tube

REFERENCES

Feng, L., & Hrnjak, P. (2017). Refrigerant Charge Imbalance in a Mobile Reversible Air Conditioning-Heat Pump System. *SAE Technical Papers*, *2017-March*(March). https://doi.org/10.4271/2017-01-0177

Finlayson, S. M., & Dickson, T. R. (2005). Accumulator sizing and evaluation technique based on theoretical optimum system performance. *SAE Technical Papers*, (724). https://doi.org/10.4271/2005-01-2048

Raiser, H., Heckenberger, T., Tegethoff, W., Köhler, J., & Försterling, S. (2006). Transient behavior of R744 vehicle refrigeration cycles and the influence of the suction side accumulator design. *SAE Technical Papers*, (724). https://doi.org/10.4271/2006-01-0162

Seeton, C. (2009). CO2-Lubricant Two-Phase Flow Patterns in Small Horizontal Wetted Wall Channels The Effects of Refrigerant. *University of Illinois at Urbana-Champaign, Dissertation*, (217).

Wang, D., Zhang, Z., Yu, B., Wang, X., Shi, J., & Chen, J. (2019). Experimental research on charge determination and accumulator behavior in trans-critical CO2 mobile air-conditioning system. *Energy*, *183*, 106–115. https://doi.org/10.1016/j.energy.2019.06.116

Wang, S., Gu, J., & Dickson, T. (2005). Model to simulate the behavior of accumulators in automotive air conditioning systems. *SAE Technical Papers*, (724). https://doi.org/10.4271/2005-01-2047

Zhang, W., & Hrnjak, P. (2020). Modeling of an Integrated Internal Heat Exchanger and Accumulator in R744 Mobile Air-Conditioning Applications. *SAE Technical Papers*, *2020-April*(April), 1–12. https://doi.org/10.4271/2020-01-0153

ACKNOWLEDGEMENT

This work was supported by Ford's University Research Project (URP) at the University of Illinois at Urbana-Champaign. All the help from Dr. Loren J Lohmeyer, Dr. Jing He, and Dr. Leyuan Yu are gratefully acknowledged!